SYNTHESIS, CHARACTERIZATION AND BIOLOGICAL EVALUATION OF SOL–GEL DERIVED NANOMATERIAL IN THE TERNARY SYSTEM 64 % SiO_2 - 31 % CaO - 5 % P_2O_5 AS A BIOACTIVE GLASS: *IN VITRO* STUDY

D. BIZARI*, M. RABIEE*, #F. MOZTARZADEH*, M. TAHRIRI*, **, S.H. ALAVI***, R. MASAELI**

**Biomaterial Group, Faculty of Biomedical Engineering (Center of Excellence), Amirkabir University of Technology, P. O. Box: 15875-4413, Tehran, Iran*
***Dental Materials Department, School of Dentistry, Tehran University of Medical Sciences (TUMS), Tehran, Iran*
****School of Mechanical and Aerospace Engineering, Oklahoma State University, Stillwater, OK 74078, USA*

#E-mail: moztarzadeh@aut.ac.ir

Submitted January 5, 2013; accepted October 6, 2013

Keywords: Bioactive glass, Sol gel, In vitro, SBF, Osteoblastic cells

In this study, we performed a new bioactive glass formulation with the molar composition 64 % SiO_2 - 31 % CaO - 5 % P_2O_5 by the sol-gel method. Sol-gel derived bioglass material was produced in nanopowder using planetary milling machine, followed by sintering at 700°C, for applications as bioactive material in bioactive scaffolds or in orthopaedic. The obtained material was evaluated by X-ray powder diffraction (XRD), thermal gravimetric analysis (TGA), differential scanning calorimetry (DSC) analyses, Fourier transform infrared spectroscopy (FTIR), scanning electron microscope (SEM) and nitrogen adsorption pore size. The biocompatibility evaluation of the formed glass was assessed through in vitro cell culture by evaluation of alkaline phosphatase activity of osteoblasts and immersion studies in simulated body fluid (SBF) for different time intervals while monitoring the pH changes and the concentration of calcium, phosphorus and silicon in the SBF medium as key factors in the rapid bonding of this bioactive glass to bone tissue as a high bioactive glass. The present investigation revealed that the sol-gel derived ternary bioglass system has the ability to support the growth of human fetal osteoblastic cells (hFOB 1.19). Finally, this material proved to be non-toxic and compatible for the proposed work in segmental defects in the goat model in vivo.

INTRODUCTION

During the last decade considerable attention has been directed towards the use of bioactive materials, where bioactivity is defined as interfacial bonding of an implant or a bioactive scaffold to tissue by means of formation of a biologically active hydroxyapatite layer on the bioactive material surface [1-3]. At present, it is possible to develop some new biomaterials due to extensive overlaps between sol-gel chemistry and biochemistry. Many kind of bioactive materials including bioglasses [4], bioglass–ceramics [5], and calcium phosphate ceramics [6], have been developed and some of them are now applied to repair and reconstruct diseased or damaged bones or tissue engineering. Bioactive materials elicit a specific biological response at the interface of the material leading to the formation of a natural bond and development of new mineralized bone tissue. Similarly bioactive glasses have been extensively studied for more than thirty years since Hench first invented Bioglass [7]. Because of the good bioactivity, osteoconductivity and biodegradability [7-9], bioglasses, as bone repair materials or fillers owing to their ability to form a bond to living bone [10], have been used in clinic for more than ten years [11-13]. Also, Hench has described a sequence of five reactions that resulted in the formation of hydroxy apatite (HA) layer on the surface of these bioactive glasses [14, 15]. A bioactive glass is one that undergoes surface dissolution in a physiological environment in order to form a hydroxycarbonate apatite (HCA) layer [16]. The larger the solubility of a bioactive glass, the more pronounced is the effect on bone tissue growth [17].

Adhesion, proliferation and differentiation are fundamental mammalian cellular processes involved in embryogenesis, immune response, tissue maintenance, and wound healing [18]. Cell contact, attachment, differentiation and subsequent adhesion of anchorage-dependent cells are among the first phases of cell–material interactions [19, 20] that soberly influence integration with tissue and eventual success or failure of a broad range of biomaterials in tissue engineering.

In this article we have tried to focus on alkaline phosphate activity of osteoblastic cells cultured on bioglass due to the fact that one of the phenotypic markers for osteoblast proliferation and differentiation is alkaline phosphatase expression which can assay by spectrophotometry. Improved hard-tissue repair, augmentation, or replacement has thus become a very significant challenge for orthopedic biomaterials and orthopedic surgery. Meeting these challenges depends, in part, on establishing firm relationships between implant success and orthopedic biomaterial properties that can guide the design process. These structure–property relationships critically depend on a thorough understanding of the adhesion of hard-tissue cells (osteoblasts, osteoclasts, chondrocytes, etc.) to artificial materials [21–23].

Various model osteoblasts have been introduced and used to gain insight into the bone–cell response to candidate orthopedic biomaterials in vitro. The most widely used model cells are primary cultures derived from normal human and rodent bone fragments, or osteosarcoma cell lines generated from human bone tumors. Each of these cell sources has strengths and limitations for studying the cell adhesion of osteoblasts in vitro [24–27]. In effort to overcome these limitations, Harris et al. [27] established a conditionally immortalized, human fetal osteoblast cell line, hFOB 1.19 that was stably transfected with a gene coding for a temperature-sensitive mutant (tsA58) of the SV40 large T antigen. Resultant hFOB cells express osteoblast-specific phenotypic markers and mineralize extracellular matrix (ECM).

In this Project, we synthesized using the sol-gel method, a bioactive glass in the ternary system with molar composition: 64 % SiO_2 - 31 % CaO - 5 % P_2O_5 (64S). There are several advantages of a sol-gel-derived glass over a melt-derived glass which are important for making bioactive materials for using in tissue engineering. Some of these merits are such as: lower temperature processing, higher bioactivity, being interconnected nanometer scale porosity consequently ability to impregnated with biologically active phases such as growth factors, higher range of SiO_2 usage (up to 90 mole %) and lack of necessity of sodium oxide which is used to conventional melt-derived bioglass [8,11]. A key feature of bioactive materials is their ability to form bone like apatite on their surfaces in vivo and in vitro. In this study Human fetal osteoblast (hFOB 1.19) cells were used for the assessment of the biocompatibility of the bioglass powder in vitro study and the hFOB cells were selected for culturing due to their relatively high growth rates and rapid differentiation into mature osteoblasts [16, 17, 28]. Also, the in vitro studies of apatite formation can carry out by soaking the glass at body temperature in an aqueous solution with pH and ionic composition similar to that of blood plasma [29]. The sequence of events leading to apatite formation includes release of ions from the glass, formation and condensation of silanol groups (Si-OH) on the glass surface, adsorption of calcium and phosphate ions to the surface to nucleate an amorphous calcium phosphate, and growth and crystallization of the calcium phosphate layer [30]. For sol-gel bioglass, the synthetic route and lower heating temperatures lead to increased numbers of silanol groups or mesopores, both of which may act as nucleation sites for apatite formation [31–35].

EXPERIMENTAL

Materials

Tetraethylorthosilicate (TEOS: $C_8H_{20}O_4Si$), calcium nitrate ($Ca(NO_3)_2.4H_2O$), and triethyl phosphate (TEP: $C_6H_{15}O_4P$) and 0.1 M nitric acid (HNO_3) and reagent-grade chemicals NaCl, $NaHCO_3$, KCl, $K_2HPO_4.3H_2O$, $MgCl_2.6H_2O$, $CaCl_2$, trishydroxy-methyl aminomethane [Tris-buffer, $(CH_2OH)_3CNH_2$], and 1 N HCl as required materials for preparation of SBF, were purchased from Merck I.

Sample Synthesis

The sol-gel-prepared glass materials SiO_2–P_2O_5––CaO (64 % SiO_2, 5 % P_2O_5, and 31 % CaO), (based on mol %), was synthesized and characterized. The solution for the glass was prepared and described as follows: 14.8 g of TEOS was added into 30 ml of 0.1 M nitric acid, the mixture was allowed to react for 30 min for the acid hydrolysis of TEOS to proceed almost to completion. The following reagents were added in sequence allowing 45 min for each reagent to react completely: 0.85 g TEP, and 7.75 g of calcium nitrate tetrahydrate. After the final addition, mixing was continued for 1 h to allow completion of the hydrolysis reaction. The solution was cast in a cylindrical Teflon container and kept sealed for 10 days at room temperature to allow the hydrolysis and a polycondensation reaction to take place until the gel was formed. The gel was kept in a sealed container and heated at 70°C for an additional 3 days. The water was removed and a small hole was inserted in the lid to allow the leakage of gases while heating the gel to 120°C for 2 days to remove all the water. Subsequently, the powders were milled by planetary milling (SVD15IG5-1, LG Company) with 400 rpm during 10 h. After grinding and sieving, the dry powder heated 24 h at 700°C for nitrate elimination. Finally the powder was ground for 10 h for achieving bioglass nanopowder.

Preparation of SBF

The SBF solution was prepared by dissolving reagent-grade NaCl, KCl, $NaHCO_3$, $MgCl_2.6H_2O$, $CaCl_2$ and KH_2PO_4 into distilled water and buffered at pH 7.25

with TRIS (trishydroxymethyl aminomethane) and HCl 1N at 37°C. Its composition is given in Table 1 and is compared with the human blood plasma [15].

Table 1. Ion concentrations of simulated body fluid (SBF) and human blood plasma.

Ion	Plasma (mmol/l)	SBF (mmol/l)
Na^+	142.0	142.0
K^+	5.0	5.0
Mg^{+2}	1.5	1.5
Ca^{+2}	2.5	2.5
Cl^-	103.0	147.8
HCO^{3-}	27	4.2
HPO_4^{-2}	1.0	1.0
SO_4^{-2}	0.5	0.5

Sample characterization

XRD analysis

The resulting powder was analyzed by X-ray diffraction (XRD) with Siemens-Brucker D5000 diffractometer. This instrument works with voltage and current settings of 40 kV and 40 mA respectively and uses Cu-Ka radiation (1.540600 Å). For qualitative analysis, XRD diagrams were recorded in the interval $10° \leq 2\theta \leq 50°$ at scan speed of 2°/min being the step size 0.02° and the step time 1 s.

TGA analysis

The thermogravimetric (TG) curve was obtained in a Shimadzu TGA-50 apparatus, under a nitrogen atmosphere that starting from room temperature up to 1200°C with the heating rate of 5°C/min.

DSC analysis

The DSC curve was obtained in a Shimadzu DSC-50 apparatus, under a nitrogen atmosphere that starting from room temperature up to 1200°C with the heating rate of 5°C/min.

FTIR analysis

The bioglass powder was examined by Fourier transform infrared spectroscopy with Bomem MB 100 spectrometer. For IR analysis, in first 1 mg of the powder samples were carefully mixed with 300 mg of KBr (infrared grade) and palletized under vacuum. Then the pellets were analyzed in the range of 500 to 4000 cm^{-1} at the scan speed of 23 scan/min with 4 cm^{-1} resolution.

SEM and EDX analysis

The morphology of the synthesized bioglass was observed by scanning electron microscopy (SEM: Philips XL30). Prior to examination, the sample was coated with a thin layer of Gold (Au) by sputtering (EMITECH K450X, England). Also, energy dispersive X-ray analyzer (EDX, Rontec, Germany) directly connected to SEM was used to investigate semiquantitatively chemical composition of the synthesized bioglass powder.

N_2 adsorption analysis

The pore texture of the sample was analyzed with an automatic nitrogen adsorption pore size analyzer (Tristar 3000, Micromeritics) by N_2 adsorption method. The samples were degassed in vacuum at 150°C for 18 - 20 h for the removal of moisture from the pores and analyzed with nitrogen adsorption. These analyses have provided the data of specific surface area, average pore size, and pore volume.

Biological properties

In vitro studies in hFOB 1.19 cells

Human fetal osteoblast cells were used for the assessment of the biocompatibility of the bioglass powder in vitro study and the hFOB 1.19 cells were selected for culturing due to their relatively high growth rates and rapid differentiation into mature osteoblasts [16–18]. We have tried to focus on alkaline phosphate activity of osteoblastic cells cultured on bioglass due to the fact that one of the phenotypic markers for osteoblast proliferation and differentiation is alkaline phosphatase expression which can assay by spectrophotometry. The alkaline phosphate (AP) activity of osteoblastic cells (hFOB 1.19) cultured on bioglass powder was studied at two different temperatures, 37°C and 39.5°C, and the results were compared with those obtained from hFOB cells cultured in polystyrene plates.

At permissive temperatures (37°C) the temperature-sensitive gene is expressed and this cell line proliferates rapidly, whereas at restrictive temperatures (39.5°C) the gene is not expressed and the cells proliferate less rapidly and express increased alkaline phosphatase activity and osteocalcin levels relative to cells cultured at the permissive temperature [36, 37]. The AP and osteocalcin are two markers of osteoblastic differentiation. Therefore some degree hFOB 1.19 proliferation and differentiation in vitro can be controlled by temperature and providing a useful model to examine the role of this kind of bioactive glass in osteoblastic differentiation. Before seeding cells the samples autoclaved at 150°C in a 95 % air and 5 % CO_2 and water-saturated atmosphere for 1 h, then cooled at room temperature, and conditioned in serum-free, sterile Dulbecco's modified Eagle's medium (DMEM) from Gibco (Grand Island, NY) (400 ml) for 24 h. The conditioned samples were seeded with 1×10^5 hFOB cells (100 µl) from a suspension containing 1.27×10^6 cells/ml. The cells were allowed to adhere to the samples in an incubator at 37°C for 60 min before the addition of 2 ml DMEM containing the nutrient F–12 (D–MEM/F12; Gibco, Gaithersburg, MD) medium supplemented with 10 % heat–inactivated fetal bovine serum (FBS)

and penicillin–streptomycin. After that for authentic comparison, the same amount of cells was seeded directly on the polystyrene plates. The medium was changed every day until day six. On day three, half of the sampless were placed in another incubator at 39.5°C to stimulate differentiation. From cultures incubated at 37°C, cells were harvested on days 3 and 6, while cultures incubated at 39°C where harvested on day 6. On day 3 and 6, the media were removed and washed twice with PBS. The cells were separated from the samples by the freeze-thaw process using the detergent Triton X100 and liquid nitrogen. The retention of osteoblastic phenotype at days 3 and 6 were evaluated by measuring alkaline phosphatase activity using a colorimetric method, and monitored by following absorption at 410 nm, and conversion to enzyme activity was made using the p-nitrophenol standard absorption curve, which is based on the conversion of p-nitrophenyl phosphate into p-nitrophenol in the presence of the alkaline phosphatase.

In vitro studies in SBF

We performed in vitro studies by soaking the samples in SBF at a concentration of 1 mg sample per milliliter of the fluid at 37°C for 5 time periods: 3 h, 1 day, 3 day, 7 and 14 days. All the reacted solution was saved for Inductively Coupled Plasma atomic emission spectroscopy (ICP-AES; Varian Co., USA) analysis of Si, Ca and P to measure ionic concentration in the SBF solution. In addition, pH of the SBF solutions were measured by a calibrated pH meter every step and using a Corning pH meter 320.

Cytotoxicity evaluation

L929 mouse fibroblast cell line (ATCC) was used for cytotoxicity. The cells were seeded in polystyrene plates enriched with Minimal Essential Medium supplemented with 10 % fetal bovine serum, 100 units/ml of penicillin and 100 µg/ml streptomycin, respectively and incubated at 37°C in humid atmosphere and 5 % CO_2. When the cells attained confluency, the sterilized bioglass block was placed in direct contact with the cells and incubated for 48 h under the same condition. Negative (Ultra High molecular weight Poly Ethylene) and positive (copper) controls were used. After 48 h, the cells were observed under optical microscopy (Nicon E200). Cellular responses were scored as 0, 1, 2 and 3 according to non-cytotoxic, mildly cytotoxic and severely cytotoxic as per ISO 10993-5.

Statistical analysis

All experiments were performed in fifth replicate. The results were given as means ± standard error (SE). Statistical analysis was performed by using One-way ANOVA and Tukey test with significance reported when $P < 0.05$. Also for investigation of group normalizing, Kolmogorov-Smirnov test was used.

RESULTS AND DISCUSSION

XRD analysis

X-ray diffraction data of the bioglass is presented on Figure 1. The XRD patterns emphasized the predominant amorphous state of the internal disorder and glassy nature of this material feature of the sample and it is worth mentioning that the bioglass does not show any crystalline states.

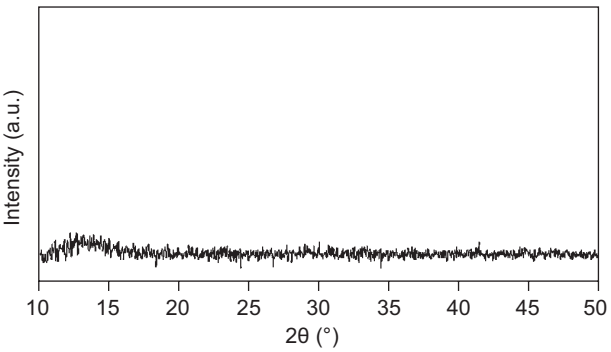

Figure 1. X-ray diffraction patterns for the bioglass nanopowder after stabilization at 700°C.

Thermal analysis

Thermogravimetric and differential scanning calorimetry of the sample were carried out to obtain the right sintering temperature. The DSC trace is a plot of heat changes of the glass as a function of temperature and is used to determine temperatures at which phase transitions occur and a TGA trace is a plot of the weight loss as a function of temperature. Figure 2 shows the TGA and DSC curves of prepared sample, dried at 70°C for 72 h and grinded. The first endothermic peak, which initiated at 55°C, corresponds to the release of physically adsorbed water that was not removed during drying. The TGA trace shows that all water and by-products from the polycondensation reaction were removed between 85°C and 150°C (17 % weight loss).

Two others endothermic peaks, starting at 380°C, corresponds to the pyrolysis reaction of free organic species and/or the release of the resulting water from the further condensation of silanol and P–OH groups and the removal of nitrate groups that are usually removed in the thermal stabilization process. The removal of species at these temperatures is reflected in the weight loss trace from TGA. All nitrates were removed by 560°C (a further 27 % of the total weight loss), so the total weight loss was 44 %. Finally, the exothermic peak around 990°C is attributed to the crystallization process of $CaSiO_3$ (β-wollastonite) and cristobalite (SiO_2) [15, 37], which has been found to form at higher temperatures in similar glasses [38, 39]. Also, a small endothermic DSC peak centralized at about 1060°C

implies that the material was fully crystalline at above 1090°C. No significant weight loss was observed above 700°C, also these curves confirmed that the residuals could be removed before 700°C, thus this temperature is appropriate for a fully stabilization of the structure. We then treated prepared sample at 700°C during 24 h for stabilization of the sample. Thereupon the XRD pattern of the prepared glass after stabilization did not contain diffraction maxima, indicative of the internal disorder and the glassy nature of this bioactive glass.

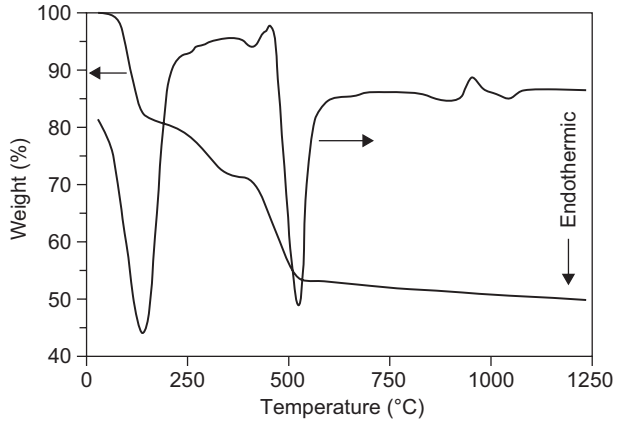

Figure 2. TGA and DSC curves of the bioglass dried at 70°C.

FTIR analysis

Figure 3 shows the FTIR spectrum, in the 500 - 4000 cm^{-1} spectral range, of sample. The bioglass nanopowder exhibited five infrared bands located at: 609, 800, 930, 1070 and 1212 cm^{-1}. Among these bands, those positioned at 800, 930, 1070 and 1212 cm^{-1} are related to the silicate network and respectively ascribed to the Si–O symmetric stretching of bridging oxygen atoms between tetrahedrons, Si–O stretching of non-bridging oxygen atoms, Si–O–Si symmetric stretching, and the LO mode of Si–O–Si asymmetric stretching. The band located at 609 cm^{-1} is attributed to the asymmetric vibration of PO_4^{3-}

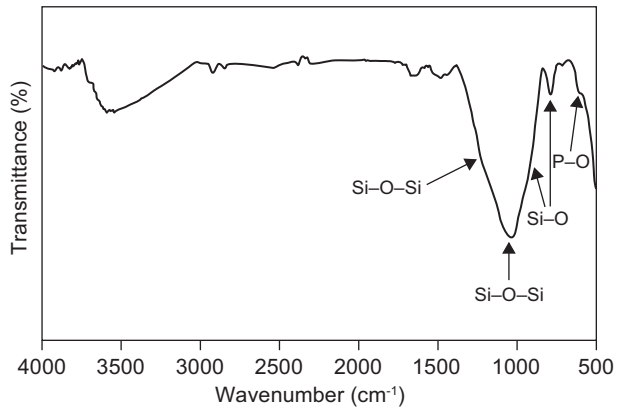

Figure 3. FTIR spectrum of the bioglass nanopowder.

Textural properties

The N_2 adsorption isotherm of the bioactive glass, shown in Figure 4 corresponds to the type IV isotherm of the Brunauer-Deming-Deming-Teller theory (BDDT) classification. From these results one can infer that the pores are in mesopores size range. The textural properties of this bioactive glass are reported in Table2.

Table 2. Textural properties of the bioactive glass.

BET Surface area (m^2 g^{-1})	Pore volume (cm^3 g^{-1})	Pore size (nm)
137.9	0.37	15.4

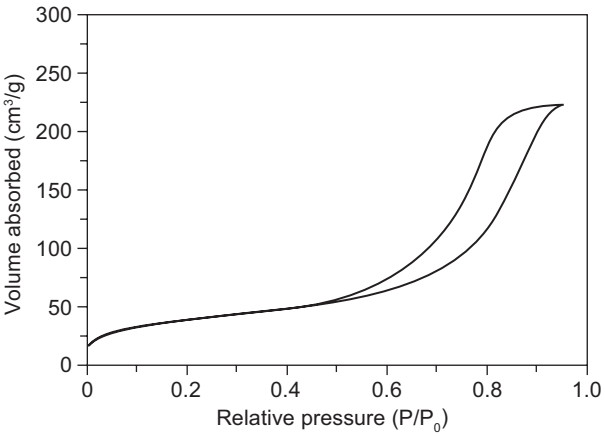

Figure 4. N_2 adsorption isotherms of the as prepared sol-gel bioglass.

SEM observations

Scanning electron microscope (SEM) was used to examine and estimate the bioglass particle size. SEM micrograph of the bioglass powder is shown in Figure 5.

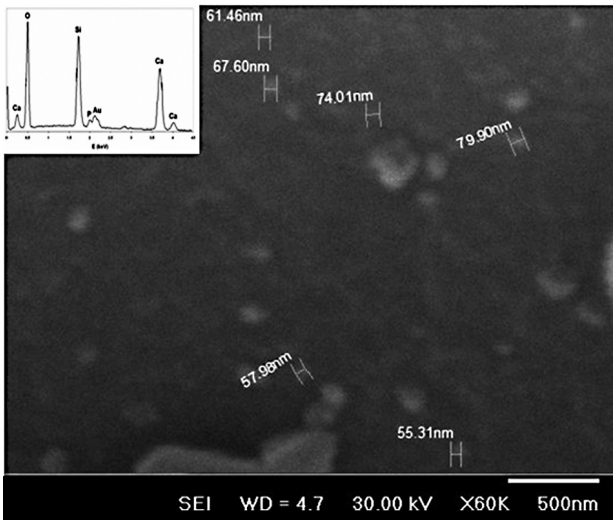

Figure 5. SEM micrograph and EDS pattern of the bioglass powder.

As it can be seen in this figure, the grain size is in the range of 50 - 100 nm. However, some agglomerated particles are probably seen that these particles can be separated easily because we ground the sample for 10 h.

Biological evaluation

Biocompatibility evaluation

The biocompatibility evaluation of the formed glass was assessed through in vitro cell culture (hFOB 1.19) experiments in this way we have tried to focus on alkaline phosphate activity of osteoblastic cells cultured on bioglass becauce one of the phenotypic markers for osteoblast proliferation and differentiation is alkaline phosphatase expression. Figure 6a-c. Present a scheme of alkaline phosphate activity at days 3 with 37°C, 6 with 37°C and 6 with 39.5°C, respectively. Statistical analysis using Student t test showed a significant difference in bone cell expression of AP activity in osteoblast culture on the samples compared with polystyrene plates ($p < 0.05$).

Figure 6a shows that the bioglass sample in this condition expressed significantly higher AP activity at day 3 for bone cell cultures at 37°C compared with bone cells cultured on polystyrene plates under the same condition. Also, we can see these results for bioglass sample at day 6 at 37°C in Figure 6b. It is noticeable that the higher AP activity of cells cultured on bioglass at 39.5°C compared with cells cultured on plates at the same temperature observed in Figure 6c. At 39.5°C the cells are supposed to proliferate less rapidly and start differentiation. At permissive temperatures (37°C) the temperature-sensitive gene is expressed and this cell line proliferates rapidly, whereas at restrictive temperatures (39.5°C) the gene is not expressed and the cells proliferate less rapidly and express increased alkaline phosphatase activity which means starting differentiation [36, 37]. The AP and osteocalcin are two markers of osteoblastic differentiation. Therefore some degree hFOB 1.19 proliferation and differentiation in vitro can be controlled by temperature and providing a useful model to examine the role of this kind of bioactive glass in osteoblastic differentiation.

A general conclusion drawn from data at hand is that the higher alkaline phosphate activity of cells grown on this bioglass at 39.5°C compared with cells grown on polystyrene plates under the same condition strongly indicate that high bioactivity in this kind of ternary system bioactive glass stimulates early bone cell differentiation. In addition gene regulation response for bone cell differentiation among surface chemistry and energy in this bioglass is incisive at early stages of cell–surface interactions and this investigation testifies that we could synthesis a high bioactive bioglass.

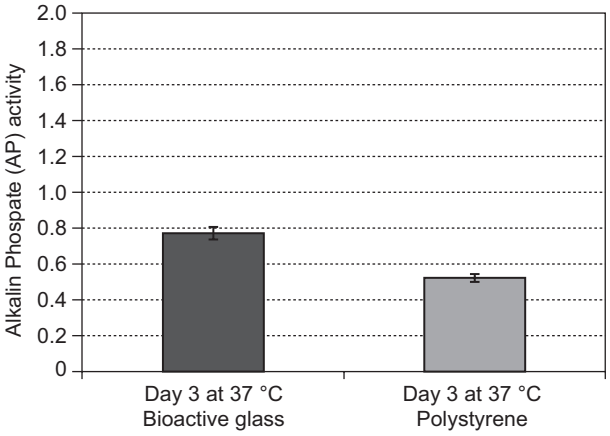

a) day 3 at 37 °C

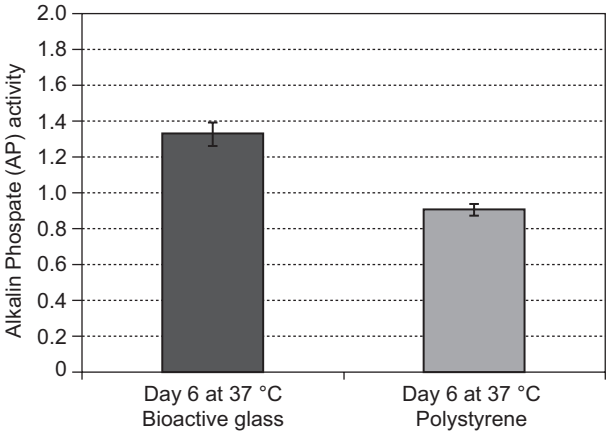

b) day 6 at 37 °C

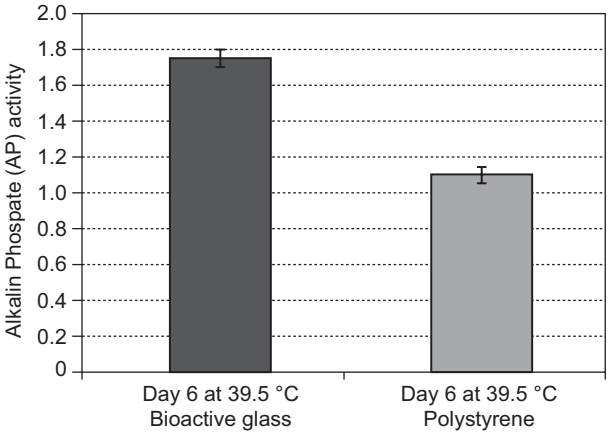

c) day 6 at 39.5 °C

Figure 6. Comparison of alkaline phosphatase activity of hFOB 1.19 cells cultured on bioactive glass powder and polystyrene plates.

Cytotoxicity evaluation

As it is seen in Figure 7, bioglass sample did not show any signs of toxicity after 48 h with L929 cells. The cells appeared spindle in shape and formed a monolayer. The cytotoxic scale was measured as zero, which corresponds to non-cytotoxicity.

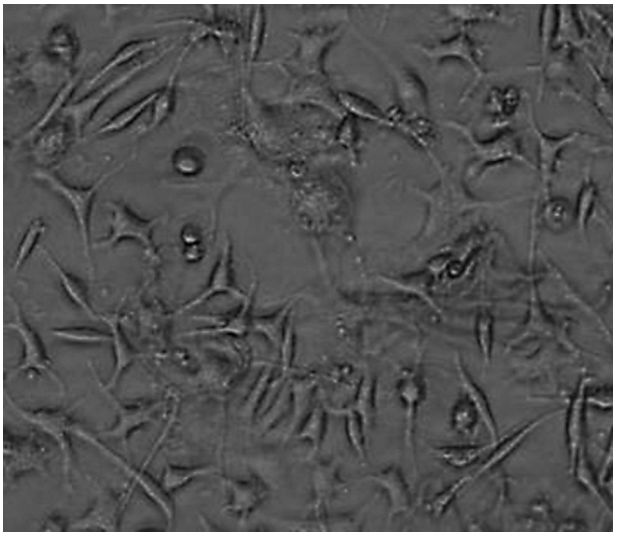

Figure 7. Optical micrograph of fibroblast cells in direct contact with bioglass.

Changes in SBF composition

Figure 8 shows the variations of Si, Ca, P concentration along with pH values in the SBF solution for various periods, measured by ICP–AES, versus soaking time, respectively. When a glass reacts with simulated body fluid (SBF), both chemical and structural changes occur as a function of time within the glass surface [42] and accumulation of dissolution products causes both the chemical composition and pH of solution to change. So with these variations we can investigate bioactivity and its mechanism in (64 % SiO_2 - 31 % CaO - 5 % P_2O_5) nanopowder bioactive glass.

As can be observed in all cases, P concentration in the solution decreased during the first hours of soaking, which shows that there was a phosphorous uptake by the glass surface and then decreased again continuously until day 3 and after that no significant change took place until day 7. In addition, pH Variation with time increased up to 8 during the first 7 days of immersion and then pH increased slowly up to 8.3 until day 14. Also Ca and Si concentrations, after a maximum at 7 days, gradually decreased up to 14 days. These changes in SBF composition are depend on 5 chemical stages in the process of formation HCA layer on the surface of ternary system bioactive glass, which Hench has described them [14, 42, 43].

In the first stage a rapid exchange between Ca^{2+} with H^+ or H_3O^+ from solution occurred, that is a diffusion

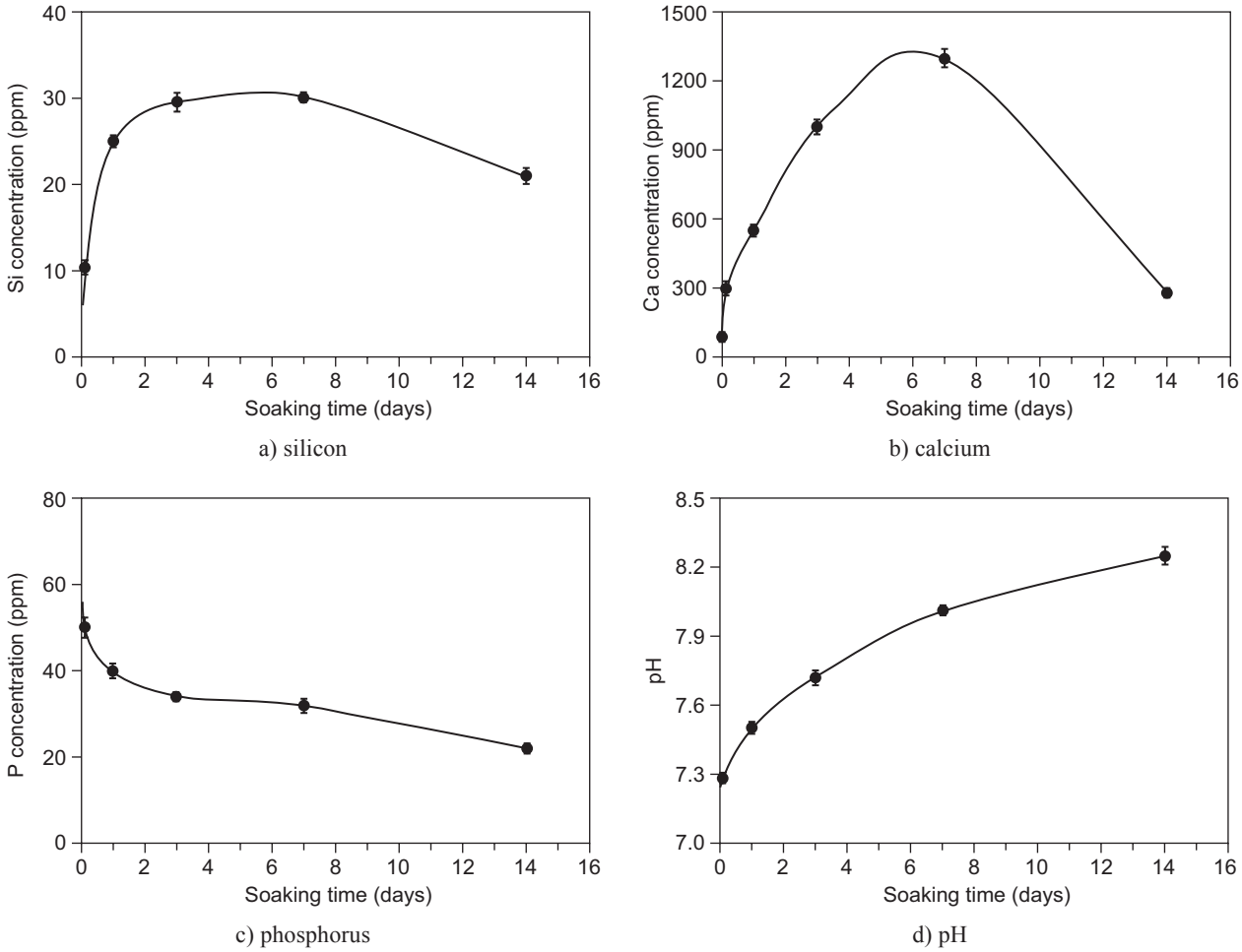

Figure 8. Variation of elemental concentration and pH in the SBF with soaking time for silicon (a), calcium (b), phosphorus (c) and pH (d).

controlled step, and causing hydrolysis of the silica groups, which creates silanol groups. When this action occurs, the pH of the solution increases, as a result of H^+ ions in the solution being replaced by cations, so we can see increasing the Ca^{2+} level with time also, the pH up to 8 during the first 7 days of immersion in SBF, which is related to control by both the release of Ca^{2+} from the bioglass nanopowder and the formation of phosphate or apatite.

In the second stage the cation exchange increases the hydroxyl concentration of the solution, which leads to attack of the silica glass network. Soluble silica is lost in the form of $Si(OH)_4$ to the solution, resulting from the breaking of Si–O–Si bonds and the continued formation of Si–OH (silanols) at the glass solution interface [44, 45]:

$$Si–O–Si + H_2O \rightarrow Si–OH + OH–Si \quad (1)$$

During 3 days that this stage on the surface of bioglass occurred, Si concentration increased up, and then no significant change took place until 7 days. When third stage occurred, Condensation and repolymerisation of a SiO_2–rich layer on the surface exhaust alkalis and alkali-earth cations. So, after a maximum at 7 days, Ca and Si concentrations gradually decreased up at 14 days. In addition, the pH level increased slowly up to 8.3 at 14 days. After that Ca^{2+} and PO_4^{3-} groups migrate to the surface through the SiO_2–rich layer, forming a CaO–P_2O_5–rich film on top of the SiO_2–rich layer, followed by growth of the amorphous CaO–P_2O_5–rich film by incorporation of soluble calcium and phosphates from solution as the fourth stage. Therefore, Ca and P ions levels changed around the day 7. The decrease in the Ca^{2+} concentration in SBF is attributed to the rapid growth of the apatite nuclei formed on surface of the glass that overcame the release rate of calcium ions to the solution [44, 45]. Finally, forming hydroxy carbonate apatite (HCA) layer occurred on the top of the bioglass surface because of crystallization of the amorphous CaO–P_2O_5 film by incorporation of OH^- and CO_3^{2-} anions from the SBF solution [45].

It is worth mentioning that the bioglass released Ca and Si ions very quickly, due to the formation of HCA on bioactive glass and the release of soluble silicon and calcium ions to the surrounding SBF environment are key factors in the rapid bonding of this nanopowder to bone tissue as a high bioactive glass [45-50].

CONCLUSION

Bioactive glass nanopowder was synthesized successfully via a sol-gel method that the processing is simple, low cost and highly efficient. The bioactive glass was performed in new formulation with the molar composition 64 % SiO_2 - 31 % CaO - 5 % P_2O_5 as a bioactive material. Thermogravimetric and differential scanning calorimetry of the sample were carried out to obtain the right sintering temperature that was 700°C. In addition, SEM micrograph of the bioglass powder is shown that the grain size of bioglass is in the nanoscale range.

For studying in vitro bioactivity in SBF, it is mentionable that the bioglass released Ca and Si ions very quickly, due to the formation of HCA on bioactive glass and the release of soluble silicon and calcium ions to the surrounding SBF environment are key factors in the rapid bonding of this nanopowder to bone tissue as a high bioactive glass. Also, a general conclusion on in vitro studies on hFOB 1.19 cells which drawn from data at hand is that the higher alkaline phosphate activity of cells grown on this bioglass at 39.5°C compared with cells grown on polystyrene plates under the same condition strongly indicate that high bioactivity in this kind of ternary system bioactive glass stimulates early bone cell differentiation. Eventually, gene regulation response for bone cell differentiation among surface chemistry and energy in this bioglass is incisive at early stages of cell–surface interactions and this investigation testifies that we could synthesis a high bioactive bioglass.

REFERENCES

1. Hench L.L., Wilson J.: *Introduction to Bioceramics*, World Scientific, Singapore, 1993.
2. Eslami H., Soalti-Hashjin M., Tahriri M.: Mater. Sci. Eng. *C 29*, 1387 (2009).
3. Hench L.L., West J.K.: Life Chem. Rep. *13*, 187 (1996).
4. Lukito D., Xue J.M., Wang J.: Mater. Let. *59*, 3267 (2005).
5. Batal H.A. E.l., Azooz M.A., Khalil E.M.A., Soltan Monem A., Hamdy Y.M.: Mater. Chem. Phys. *80*, 599 (2003).
6. Navarro M., del Valle S., Martínez S., Zeppetelli S., Ambrosio L., Anton Planell J., Ginebra M.P.: Biomaterials *25*, 4233 (2004).
7. Hench L.L., Splinter R.J., Allen W.C., Greenlee T.K.: J. Biomed Mater. Res. *2*, 117 (1971).
8. Hench L.L.: Curr. Orthop. *14*, 7 (2000).
9. Wilson J., Low S.B.: J. Appl. Biomater. *3*, 123 (1992).
10. Vallet-Regi M., Ragel C.V., Salinas A.J.: J. Inorg. Chem. *21*, 1029 (2003).
11. Hench L.L., West J.K.: Life Chem. Rep. *13*, 187 (1996).
12. Hench L.L., Xynos I.D., Polak J.M.: J. Biomater. Sci. Polym. Ed. *15*, 543 (2004).
13. Hench L.L.: J. Am. Ceram. Soc. *74*, 1487 (1991).
14. Hench L.L., LaTorre G.P.: Bioceram. *5*, 67 (1993).
15. Saboori A., Rabiee M., Moztarzadeh F., Sheikhi M., Tahriri M., Karimi M.: Mater. Sci. Eng. *C 29*, 335 (2009).
16. Popat K.C., Leary Swan E.E., Mukhatyar V., Chatvanichkul K.I., Mor G.K., Grimes C.A.: Biomaterials *26*, 4516 (2005).
17. Montjovent M.O., Burri N., Mark S., Federici E., Scaletta C., Zambelli P.Y.: Bone *35*, 1323 (2004).
18. Baxter L.C., Frauchiger V., Textor M., Gwynn I., Richards R.G.: Eur. Cells Mater. *4*, 1 (2002).
19. Grinnell F. in: *International review of cytology*, p. 67–145, Eds. Bourne G.H., Danielli J.F., Jeon K.W., Academic Press, New York, 1978.
20. Altankov G., Grinnell F., Groth T.: J. Biomed. Mater. Res. *30*, 385, (1996).

21. Kiberstis P., Smith O., Norman C.: Science *289*, 1497 (2000).
22. Rodan G.A., Martin T.J.: Science *289*, 1508 (2000).
23. Service R.F.: Science *289*, 1498 (2000).
24. Keeting P.E., Scott R.E., Colvard D.S., Anderson M.A., Outsler M.J., Spelsberg T.C., et al.: J. Bone Miner. Res. *7*, 127 (1992).
25. Clover J., Gowen M.: Bone *15*, 585 (1994).
26. Harris S.A., Enger R.J., Riggs B.L., Spelsberg T.C.: J. Bone Miner. Res. *10*, 178 (1995).
27. Liua X., Limb J. Y., Donahueb H.J., Dhurjatic R., Mastrod A.M., Vogler E.A.: Biomaterials *28*, 4535 (2007).
28. Subramaniam M., Jalal S.M., Rickard D.J., Harris S.A., Bolander M.E., Spelsberg T.C.: J. Cell Biochem. *87*, 9 (2002).
29. Kokubo T., Kushitani H., Sakka S., Kitugi T., Yamanuro T.: J. Biomed. Mater. Res. *24*, 721 (1990).
30. Hench L.L.: J. Am. Ceram. Soc. *81*, 1705 (1998).
31. Li R., Clark A.E., Hench L.L.: *Chemical processing of advanced materials*, John Wiley and Sons, New York, 1992.
32. Li P., Ohtsuki C., Kokubo T., Nakanishi K., Soga N.: J. Am. Ceram. Soc. *75*, 2094 (1992).
33. Li P., Ohtsuki C., Kokubo T., Nakanishi K., Soga N., de Groot K.: J. Biomed. Mater. Res. *28*, 7 (1994).
34. Pereira M.M., Clark A.E., Hench L.L.: J. Am. Ceram. Soc. *78*, 2463 (1995).
35. Pereira M.M., Hench L.L.: J. Sol-Gel Sci. Tech. *7*, 59 (1996).
36. Ducy P., Karsentry G.: Curr. Opin. Cell Biol. *10*, 614 (1998).
37. Saravanapavan P., Jones J.R., Pryce R.S., Hench L.L.: J. Biomed Mater. Res. *A 66*, 110 (2003).
38. Jones J.R., Ehrenfried L.M., Hench L.L.: Biomaterials *27*, 964 (2006).
39. Roman J., Padilla S., Vallet-Regi M.: Chem. Mater. *15*, 798 (2003).
40. Mami M., Lucas-Girot A., Oudadesse H., Dorbez-Sridi R., Mezahi F., Dietrich E.: Appl. Surf. Sci. *254*, 7386 (2008).
41. Vidueau J.J., Dupius V.: Eur. J. Solid State Inorg. Chem. *28*, 303 (1991).
42. Clark A.E., Pantano C.G., Hench L.L.: *Corrosion of glass*, Magazines for Industry, New York, 1979.
43. Hench L.L., Polak J.M.: Science *295*, 1014 (2002).
44. Martinez A., Izquierdo-Barba I., Vallet-Regi M.: Chem. Mater. *12*, 3080 (2000).
45. Polak J.M., Hench L.L., Kemp P. in: *Bioactive materials for tissue engineering scaffolds*, p. 1–22, Eds. Hench L.L., Jones J.R., Sepulveda P., Imperial College Press, London, 2002.
46. Greenspan D.C., Zhong J.P., LaTorre G.P. in: Bioceramics *7*, p. 28–33, Eds. Andersson O.H., Yli-Urpo A., 1994.
47. Greenspan D.C., Zhong J.P., Chen Z.F., LaTorre G.P.: Bioceramics *10*, 391 (1997).
48. Greenspan D.C., Zhong J.P., Wheeler D.L.: Bioceramics *11*, 345 (1998).
49. Fu H., Fu Q., Zhou N., Huang W., Rahaman M.N., Wang D., Liu X.: Mater. Sci. Eng. *C 29*, 2275 (2009).
50. Jones J.R.: J. Eur. Ceram. Soc. *29*, 1275 (2009).